

# Blue horizontal branch stars in the Sloan Digital Sky Survey: II. Kinematics of the Galactic halo

Edwin Sirko<sup>1</sup>, Jeremy Goodman<sup>1</sup>, Gillian R. Knapp<sup>1</sup>, Jon Brinkmann<sup>2</sup>, Željko Ivezić<sup>1</sup>,  
Edwin J. Knerr<sup>1,3</sup>, David Schlegel<sup>1</sup>, Donald P. Schneider<sup>4</sup>, Donald G. York<sup>5</sup>

## ABSTRACT

We carry out a maximum-likelihood kinematic analysis of a sample of 1170 blue horizontal branch (BHB) stars from the Sloan Digital Sky Survey presented in Sirko et al. (2003) (Paper I). Monte Carlo simulations and resampling show that the results are robust to distance and velocity errors at least as large as the estimated errors from Paper I. The best-fit velocities of the Sun (circular) and halo (rotational) are  $245.9 \pm 13.5 \text{ km s}^{-1}$  and  $23.8 \pm 20.1 \text{ km s}^{-1}$  but are strongly covariant, so that  $v_{\odot} - v_{\text{halo}} = 222.1 \pm 7.7 \text{ km s}^{-1}$ . If one adopts standard values for the local standard of rest and solar motion, then the halo scarcely rotates. The velocity ellipsoid inferred for our sample is much more isotropic  $[(\sigma_r, \sigma_{\theta}, \sigma_{\phi}) = (101.4 \pm 2.8, 97.7 \pm 16.4, 107.4 \pm 16.6) \text{ km s}^{-1}]$  than that of halo stars in the solar neighborhood, in agreement with a recent study of the distant halo by Sommer-Larsen et al. (1997). The line-of-sight velocity distribution of the entire sample, corrected for the Sun's motion, is accurately gaussian with a dispersion of  $101.6 \pm 3.0 \text{ km s}^{-1}$ .

*Subject headings:* Galaxy: halo — Galaxy: kinematics and dynamics — stars: horizontal branch

## 1. Introduction

Among all visible components of the Galaxy, the stellar halo is the oldest and occupies the largest volume. It is therefore of interest both as a record of the early history of the Galaxy and as a tracer of the Galactic potential.

The kinematics of halo stars in the solar neighborhood are well established, as shown in Table 1. For present purposes, the solar neighborhood extends as far as a few kpc from the Sun, but to a

---

<sup>1</sup>Princeton University Observatory, Princeton, NJ 08544

<sup>2</sup>Apache Point Observatory, P.O. Box 59, Sunspot, NM 88349

<sup>3</sup>Law School, University of Minnesota, Minneapolis, MN 55455

<sup>4</sup>Department of Astronomy and Astrophysics, the Pennsylvania State University, University Park, PA 16802

<sup>5</sup>Department of Astronomy and Astrophysics, University of Chicago, 5640 South Ellis Avenue, Chicago, IL 60637

distance less than the Sun’s own Galactocentric radius. Evidently, the systemic rotation  $v_{\text{halo}}$  of the local halo is small or zero, and the velocity ellipsoid is distinctly elongated in the radial direction.

The more distant halo has been less well studied. Proper motions are generally not measurable for distant stars, so that line-of-sight velocities must be analyzed under *a priori* assumptions about the symmetries of the velocity ellipsoid. The stars are also fainter, reducing the accuracy of the measured quantities.

Much work on the distant halo has been done using globular clusters, which have the advantage of being distinctive and bright, but have important drawbacks: there are only  $\sim 10^2$  of them, so that statistical uncertainties are large, and special conditions of formation or selective destruction by Galactic tides may have biased the properties of the cluster system compared to those of the field. Frenk & White (1980) analyzed the kinematics of a sample of 66 globular clusters under the assumption that the systemic rotation  $v_{\text{halo}}$  is constant; they concluded that the residual velocities are consistent with being isotropic within broad uncertainties. For a subsample of 44 metal-poor (“F”) clusters, they found  $v_{\text{halo}} = 42 \pm 33 \text{ km s}^{-1}$  and a root-mean-square (rms) residual line-of-sight velocity  $\sigma_{\text{los}} = 124 \text{ km s}^{-1}$ . In a similar analysis of clusters with  $[\text{Fe}/\text{H}] < -0.8$ , Armandroff (1989) found  $v_{\text{halo}} = 46 \pm 29 \text{ km s}^{-1}$  and  $\sigma_{\text{los}} = 116 \pm 10 \text{ km s}^{-1}$ . The restriction to low metallicities follows the discovery by Zinn (1985) that the more metal-rich clusters have a distribution and kinematics intermediate between those of the stellar halo and thin disk.

Ratnatunga & Freeman (1989) sampled the halo field using relatively faint red giants at high Galactic latitude. Their summary for the more metal-poor stars near the south Galactic pole concludes that  $\sigma_z$  is approximately constant at  $\sim 75 \text{ km s}^{-1}$  out to 25 kpc, which would be consistent with the solar neighborhood (Table 1) if the velocity ellipsoid is constant in cylindrical coordinates; however, for their most distant subsample near the SGP ( $\langle D \rangle = 17.1 \text{ kpc}$ ), they measured  $\sigma_{\text{los}} = 42 \pm 10$  (10 stars).

In a study similar to that reported here, Sommer-Larsen et al. (1997) analyzed a sample of 679 blue horizontal branch stars drawn from multiple sources and spanning Galactocentric radii  $\sim 7 - 65 \text{ kpc}$ . With line-of-sight velocities and photometric distances, they found that the radial velocity dispersion (in spherical coordinates) falls rather sharply from its value in the solar neighborhood,  $\sigma_r = 140 \pm 10 \text{ km s}^{-1}$ , to an asymptotic value  $89 \pm 19 \text{ km s}^{-1}$  at  $r \gtrsim 20 \text{ kpc}$ . By requiring dynamical equilibrium in an assumed logarithmic Galactic potential, they concluded that the tangential velocity dispersion should rise from its local value to  $\sigma_\theta \approx \sigma_\phi \approx 137 \text{ km s}^{-1}$  at large  $r$ . They did not claim, however, to have detected this rise directly in their data. They further suggested that the shift from radial to tangential anisotropy with increasing Galactocentric radius might support theories in which the halo formed by heirarchical merging of smaller systems.

Because of the differences in kinematics cited above, it appears that local high-velocity, low-metallicity stars may not be entirely representative of the more distant halo. To study the more distant halo, we have isolated a sample of 1170 blue horizontal branch (BHB) stars from the Sloan Digital Sky Survey (Sirko et al. 2003, hereafter Paper I). In that paper, we estimated contamination

from foreground stars and blue stragglers to be less than 10% for bright stars ( $g < 18$ ) and about 25% for faint stars ( $g > 18$ ). An improved color-absolute magnitude relation was also derived, and these absolute magnitudes are used throughout this paper to derive distance moduli. This sample of BHB stars provides effective tracers of the Galactic halo, with no kinematic bias. The sample may have selection bias, and is probably far from complete, but these biases do not affect the kinematic analyses presented in this paper other than degrading the statistics and increasing the errors. Using maximum-likelihood methods, we fit for the mean rotation and principle axes of the halo velocity ellipsoid on the assumption that these are constant in spherical or cylindrical coordinates. We also fit for the orbital velocity of the Sun.

The present paper is organized as follows. We first discuss an overview of the kinematic analysis in §2 and appendix A. The results for the kinematic parameters of the halo are presented in §3 and summarized in Table 2. Monte Carlo simulations which validate the analysis are presented in §4. §5 summarizes our main conclusions and discusses the agenda for future work.

### 1.1. Terminology used in this paper

The following terminology and conventions are used throughout this work. A heliocentric right-handed Cartesian coordinate system  $(x, y, z)$  is oriented so that  $+x$  points towards the Galactic center (GC) and  $+z$  points towards the North Galactic Pole, such that  $+y$  is the direction of disk rotation. Thus,  $\mathbf{v}_\odot = (v_{\odot,x}, v_{\odot,y}, v_{\odot,z}) = \mathbf{v}_{\text{LSR}} + (U, V, W)$  where  $(U, V, W)$  is the solar motion with respect to the local standard of rest (LSR). The velocity of the LSR is taken to be  $\mathbf{v}_{\text{LSR}} = (0, 220, 0) \text{ km s}^{-1}$  (Kerr & Lynden-Bell 1986), and the canonical solar motion vector is  $(U, V, W) = (10, 5, 7) \text{ km s}^{-1}$  (Dehnen & Binney 1998, rounded to integer values). Galactocentric spherical  $(r, \theta, \phi)$  and cylindrical  $(R, \phi, z)$  coordinate systems will also be used. We make a rudimentary model of halo bulk rotation parametrized by a single velocity  $v_{\text{halo}}$ . A positive  $v_{\text{halo}}$  indicates a flat halo rotation curve in the same sense as the disk rotation. Radial velocities to stars are measured as redshifts which are subsequently and immediately corrected for the Earth’s motion around the Sun and the Earth’s rotation about its own axis. This heliocentric radial velocity  $v_r$  contains a component due to the solar velocity  $\mathbf{v}_\odot$ .<sup>6</sup> The “line-of-sight” velocity  $v_{\text{los}}$  will be defined as  $v_r$  plus the projection of  $\mathbf{v}_\odot$  onto the line-of-sight to the star, minus the projection of its expected rotation component  $-v_{\text{halo}}\hat{\phi}$  (if any). That is,  $v_{\text{los}}$  is the component of the purely random component of velocity in a model of the halo with a flat rotation curve, projected onto the line of sight. We find  $v_{\text{los}}$  conceptually useful, but one should not forget that it is contingent upon our assumptions concerning the rotation of the Sun and the halo, whereas  $v_r$  is directly observed (modulo errors). Throughout, the distance from the Sun to the GC is assumed to be 8 kpc (Reid 1993).

---

<sup>6</sup>Here the subscript “ $r$ ” is used for components along the line of sight, but elsewhere it will be used for the radial component in spherical coordinates based on the Galactic Center. The context should make our meaning clear.

## 2. The velocity ellipsoid of the Galactic halo: overview

The velocity ellipsoid is defined such that its axes align with the principal axes of the velocity dispersion tensor, and the lengths of its axes  $\sigma$  are equal to the components of the velocity dispersion along those directions. It is difficult to know the orientation of the velocity ellipsoid so it is reasonable to assume it is oriented along galactocentric spherical or cylindrical coordinates at every point in space (Binney & Merrifield 1998). Even with  $\sim 10^3$  stars, it is difficult to assess whether and how the components of the velocity ellipsoid vary in space, so they are assumed constant, although we test this below by dividing our sample into a few magnitude bins.

A maximum likelihood technique is used, as outlined in Appendix A. A uniform prior is adopted (Lupton 1993): when the probability of observing the set of stars at the observed positions and heliocentric radial velocities given an assumed  $\sigma$  is maximized as a function of  $\sigma$ , the probability of  $\sigma$  being the true velocity ellipsoid is maximized. In symbols,  $\phi(v_{\text{los}} | \sigma) \propto \phi(\sigma | v_{\text{los}})$  where  $\phi$  represents probability density. Naturally,  $\phi(v_{\text{los}} | \sigma)$  depends implicitly upon the orientation of the velocity ellipsoid with respect to the line of sight, and hence upon the angular position  $(\alpha, \delta)$  and distance of each star. It is straightforward to expand the maximum likelihood procedure to include four additional parameters: the three components of the velocity of the Sun with respect to the galactic center,  $\mathbf{v}_{\odot}$ , and the bulk rotation velocity of the halo,  $v_{\text{halo}}$ .

We assume that the bulk rotation of the halo corresponds to a uniform velocity in the direction of galactic rotation. It is difficult to apply this analysis on this sample to more complex halo rotation laws because of the moderate degeneracy between the halo rotation and  $v_{\odot,y}$  (see figure 2, discussed below); this degeneracy would increase if one attempted to fit for more parameters of the bulk halo rotation.

Distance moduli are derived from the color-absolute magnitude relation of Paper I. The measured angular coordinates of the stars  $(\alpha, \delta)$  are virtually error-free. However, the magnitudes, and thus distances, are susceptible to several sources of error: extinction, photon statistics, and intrinsic brightness variations from star to star which create deviations in the stars' distance moduli. Therefore, magnitude errors should be included in the likelihood analysis. As shown in Paper I, typical magnitude errors are about  $\Delta m \sim 0.2$ . In anticipation of our finding, discussed below in §3, that the kinematic analysis is very robust with respect to magnitude errors, we adopt an even more conservative magnitude error:  $\Delta m = 0.5$ , and assume the errors follow a gaussian distribution. Equation A3 shows the probability density  $\phi$  of observing a star at a given position in space, line of sight velocity  $v_{\text{los}}$ , and  $\sigma$ . Having assumed that magnitude errors have a gaussian distribution with some width  $\Delta m$ , the likelihood of observing a star considering magnitude errors can be found by integrating the probability density of equation A3, multiplied by a gaussian weight function for the magnitude error, along the line of sight. Figure 1 shows an illustration of this procedure for two stars with artificial data. These two stars are constructed to have  $(l, b) = (0, 30)$ ,  $g = 15.5$ , and absolute magnitude 0.7, which places them approximately 9 kpc from the Sun above the galactic center. The evaluation of the probability density  $\phi$  for each star alone along the line

of sight is shown in the upper right panel. One star’s line-of-sight velocity is  $v_{\text{los}} = 0 \text{ km s}^{-1}$  (solid line and filled dots) and the other’s is  $v_{\text{los}} = 100 \text{ km s}^{-1}$  (dotted line and open circles). We apply  $\sigma = (150, 50, 100) \text{ km s}^{-1}$  (spherical coordinates) to this model (note that the  $\phi$  component of the velocity ellipsoid is irrelevant for this particular case). It is easy to see several trends in the upper right plot of figure 1. If there were no distance measurement, for example, the stationary star would be most likely to be found at  $\approx 7 \text{ kpc}$  because the line of sight coincides there with the smallest ( $\theta$ ) axis of the velocity ellipsoid. In fact, the probability density of observing a stationary star at that point is just  $(2\pi\sigma_\theta^2)^{-1/2} \approx .008 \text{ s km}^{-1}$ , as shown. Also, the receding star is least likely to be observed there because its  $v_{\text{los}}$  can most easily be “explained” by most of its contribution coming from the radial component of the velocity ellipsoid. Also note that the stationary star always has a higher probability than the receding star; this follows from the gaussian nature of the probability of observing  $v_{\text{los}}$  in equation A3.

To incorporate the magnitude error  $\Delta m$  into the analysis, the probability density  $\phi$  as a function of distance must be multiplied by a gaussian centered on the measured magnitude with width  $\Delta m$ , and then integrated over distance. This integration is most easily accomplished with Gauss-Hermite integration, which samples  $\phi$  at  $N_p = 11$  points, shown in the upper right panel of figure 1 as dots and circles. These 11 values of  $\phi$  at the specified abscissae are multiplied by the corresponding weight factors  $w_j$  (Abramowitz & Stegun 1972), which are plotted in a discrete fashion as the lower line in the middle panel of figure 1. The consideration of magnitude errors also introduces Malmquist bias. If the number density of observable BHB stars in the Galactic halo follows a spherical power law  $\rho \propto r^{-\alpha}$  in Galactocentric radius, then Malmquist factor  $M(r') \propto r'^3 r^{-\alpha}$  must weight the probability density  $\phi$ , in addition to the gaussian weight  $w_j$  due to the magnitude error, where  $r'$  is heliocentric distance. These weighting factors are normalized so that  $\sum_j^{N_p} w_j M(r) = 1$ . The function  $M(r')$  is shown in the middle panel of figure 1 as the top line, assuming  $\alpha = 3.5$ . Note that for  $\alpha = 3$ ,  $M(r \gg 8 \text{ kpc}) \rightarrow \text{constant}$ .

Finally, the probability density of observing a star at a given angular position, distance modulus, and line-of-sight velocity, with assumptions on  $\sigma$ ,  $\Delta m$  and  $\alpha$  for the Malmquist term, is just  $\sum_j \phi(r) w_j M(r)$ . The term  $\phi(r) w_j M(r)$  is plotted in the lower panel of figure 1 for our two fictitious stars; again the stationary star is the solid line and the receding star is the dotted line. When these terms are summed over  $j$ , we arrive at new determinations for the probability density of observing the star, indicated in the upper right panel of figure 1 by the horizontal lines. The original estimate of  $\phi$  was given by the middle dot and circle (at  $\approx 9 \text{ kpc}$ ), so it is evident that the “hill” and the “dip” in  $\phi(r)$  for the two stars are responsible for modifying the original estimate of  $\phi$  up or down in the correct direction.

The quantity  $\alpha$  for the halo is usually taken to be between about 3 and 3.5 (Yanny & Newberg et al. 2000, and references therein). In the kinematic analysis below we assume  $\alpha = 3.5$ , following the study of horizontal branch stars of Kinman, Suntzeff, & Kraft (1994). However, we find our results are fairly insensitive to  $\alpha$ ; even  $\alpha = 10$  results only in small changes to our final results.

Another possible source of measurement error is in the radial velocities. As determined in Paper I, typical velocity errors may be as high as  $\sim 30 \text{ km s}^{-1}$ . According to equation A3, the probability density of observing a star at a certain line-of-sight velocity  $v_{\text{los}}$  (with respect to the GC) follows a gaussian distribution, centered on  $v_{\text{los}} = 0 \text{ km s}^{-1}$ , with a dispersion  $\hat{\sigma}_{\text{los}}$  that depends on geometry and  $\sigma$ . Thus the probability density of observing the star at  $v_{\text{los}}$  considering a possible velocity error that follows a gaussian distribution with dispersion  $\Delta v$  is just

$$\begin{aligned} \phi_e(v_{\text{los}}) &= \frac{1}{\Gamma \sqrt{2\pi\Delta v^2}} \int_{-\infty}^{\infty} \exp\left(\frac{-v^2}{2\hat{\sigma}_{\text{los}}^2} - \frac{(v - v_{\text{los}})^2}{2\Delta v^2}\right) dv \\ &= \frac{1}{\Gamma \sqrt{1 + (\Delta v/\hat{\sigma}_{\text{los}})^2}} \exp\left(\frac{-v_{\text{los}}^2}{2(\hat{\sigma}_{\text{los}}^2 + \Delta v^2)}\right); \end{aligned} \quad (1)$$

note this reduces to the original equation A3 as  $\Delta v \rightarrow 0$ .

We have discussed the various modifications available to the maximum likelihood technique. In summary, they are the following:

- **Subsample.** Although we first determine the velocity ellipsoid using all stars, we can extract subsamples, specifically in certain magnitude bins, to investigate whether the velocity ellipsoid is a function of position in space.
- **Spherical or cylindrical coordinates.** The choice affects the values of  $\mathbf{x}$  in the maximum likelihood procedure but is otherwise straightforward.
- **Magnitude errors.** We either ignore magnitude errors or else use 11-point Gauss-Hermite integration with  $\Delta m = 0.5$  and  $\alpha = 3.5$ .
- **Velocity errors.** We either ignore velocity errors or else use equation 1 with  $\Delta v = 30 \text{ km s}^{-1}$ .
- **Number of fitting parameters.** Several combinations of fitting parameters are used. We fit the three  $\sigma$  parameters keeping  $(\mathbf{v}_{\odot}, v_{\text{halo}})$  at canonical values; we fit  $(v_{\text{halo}}, \sigma)$  keeping  $\mathbf{v}_{\odot}$  at its canonical values; and we also fit all seven parameters simultaneously.

### 3. Results

Table 2 contains the determinations of  $(\mathbf{v}_{\odot}, v_{\text{halo}}, \sigma)$  for several combinations of model assumptions discussed above; the first four columns describe these model assumptions. The first column states what criteria were used to select subsets of BHB stars from the total set of 1170 BHB stars, and the number of stars in each subset is listed in the second column. The third column indicates whether a cylindrical or spherical geometry was assumed. The fourth column indicates how errors were handled; “0” indicates that errors were not considered. As described in §2, “m” indicates that 11-point Gauss-Hermite integration was used with  $\Delta m = 0.5$ , and “v” indicates that velocity errors were considered with  $\Delta v = 30$ . The following columns show the parameter determinations. All

determinations in table 2 are for the three-parameter fit with  $(\mathbf{v}_\odot, v_{\text{halo}})$  fixed at canonical values (Dehnen & Binney 1998) as shown, except for the second and third lines which fit four and seven parameters, respectively. The quoted errors consider correlations among the parameters, and the errors in parentheses do not consider the correlations. The former error is defined as  $\sqrt{-W_i/2}$  and the latter as  $1/\sqrt{-2M_i}$  where  $M_i$  represents the diagonal elements of the second-derivative matrix of the log-likelihood function, and  $W_i$  represents the diagonal elements of the inverse of that matrix.

The first row in Table 2 shows the results for the velocity ellipsoid for the complete sample ( $N_{\text{stars}} = 1170$ ) in spherical coordinates, with no magnitude or velocity errors considered. The Sun’s velocity was fixed at the canonical value of  $\mathbf{v}_\odot = \mathbf{v}_{\text{LSR}} + (U, V, W) = (0, 220, 0) + (10, 5, 7) \text{ km s}^{-1}$  (Dehnen & Binney 1998). Under these assumptions all three components of the velocity ellipsoid are about  $100 \text{ km s}^{-1}$ . The second row in Table 2 shows the results of simultaneously fitting  $v_{\text{halo}}$  and  $\sigma$  to the same sample and otherwise same set of assumptions discussed above. The velocity ellipsoid has essentially the same determined values, and the rotation velocity of the halo is consistent with zero. The third row in Table 2 is the seven parameter fit to the sample. Again, the velocity ellipsoid is essentially the same, and the rotation velocity of the halo is seen to be marginally consistent with zero. Reassuringly, the velocity of the Sun with respect to the galactic halo in the  $y$  direction (or equivalently, the Sun’s velocity in an inertial frame assuming the halo is actually non-rotating) is close to the expected value:  $v_{\odot,y} - v_{\text{halo}} = 222.1 \pm 7.7 \text{ km s}^{-1}$ . The error follows from rotating the eigenvectors by 45 deg and is smaller than either error for  $v_{\odot,y}$  or  $v_{\text{halo}}$  because the two quantities are strongly covariant. The  $x$  and  $z$  directions of  $\mathbf{v}_\odot$  are new measurements of the solar motion  $(U, W)$ . Our value of  $U$  is consistent with that of Dehnen & Binney (1998); however our value of  $W$  differs by several  $\sigma$ .

Figure 2 shows confidence regions for the components of the velocity ellipsoid for this case. Each panel in figure 2 is a two-dimensional parameter space where the other five parameters are held at their determined values and assumed to have symmetric errors, so the confidence regions are only approximations to those one would obtain by integrating over the other five dimensions. Note that  $\sigma_r$  is very well constrained. This is because the typical distance to the halo stars in our sample is large compared to the distance from the Sun to the galactic center, so measurements of  $v_{\text{los}}$  from Earth very nearly align with direct measurements of the galactocentric radial component of velocity. Also, each component of the velocity ellipsoid is anticorrelated with the other two; this demonstrates an intuitive “conservation law” of velocities. In the lower left panel, it is apparent that  $v_{\text{halo}}$  and  $v_{\odot,y}$  are correlated, so that the quantity  $v_{\odot,y} - v_{\text{halo}}$  is more tightly constrained than either quantity alone. This of course follows from the reasonable assumption that the halo rotation at the location of the Sun is in the  $y$  direction.

The result that  $\sigma_r \approx 100 \text{ km s}^{-1}$  contrasts with most estimates of the velocity ellipsoid based on stellar samples in the solar neighborhood (Woolley 1978; Pier 1984; Carney & Latham 1986; Norris 1986; Layden et al. 1996). We now investigate some other sets of assumptions that may influence the results.

The fourth line in Table 2 introduces magnitude errors into the set of assumptions. These errors, at least in our implementation of a gaussian with width  $\Delta m = 0.5$ , apparently have little effect on the final results. Note that for a given kinematic model, distance affects the distribution of  $v_{\text{los}}$  only through the orientation of the velocity ellipsoid with respect to the line of sight. If the dispersions were isotropic and the halo nonrotating, which seem to be nearly the case, then  $v_{\text{los}}$  would be independent of distance. This may explain the insensitivity to magnitude errors. The fifth line in Table 2 incorporates both magnitude and velocity errors. Again, the final results are seen to remain relatively constant; however the values of the velocity ellipsoid components decrease modestly. In light of equation A3, the probability of observing a star at a certain velocity  $v_{\text{los}}$  is always higher for smaller values of  $|v_{\text{los}}|$ ; thus velocity errors tend to “favor” smaller velocities, which propagate to the smaller values of the velocity ellipsoid. However, the effect is small, of order  $\sqrt{\sigma^2 + \Delta v^2} - \sigma \approx 5 \text{ km s}^{-1}$ .

The next three lines in Table 2 show three-parameter determinations for the complete sample of BHB stars assuming the velocity ellipsoid is oriented along cylindrical coordinates. As for the spherical coordinates case, all three components of the velocity ellipsoid are still about  $100 \text{ km s}^{-1}$ .

Determinations for cylindrical scenarios incorporating magnitude and velocity errors are shown in the tables, and as before, do not appear to affect the final results appreciably. Since velocity errors behave in a predictable way and have little effect on our final results, and magnitude errors have no noticeable effect, we do not consider these errors further. It should be remembered that our error estimate was based on a set of highly simplified, and perhaps dubious, assumptions that do not take into account systematic errors, for instance.

In the following rows in Table 2 the sample of stars is modified. There are 733 stars with  $g < 18$ , so these stars extend from  $\sim 7 \text{ kpc}$  to  $\sim 30 \text{ kpc}$ . The sample with  $g < 16$  contains the 227 brightest stars (distances out to  $11.5 \text{ kpc}$ ). The velocity ellipsoid is seen to remain remarkably constant down to distances from the Sun only marginally outside the coverage of previous surveys (e.g.,  $V \lesssim 13$  for the sample of Layden et al. (1996)). The most intriguing result is that the radial component of the velocity ellipsoid  $\sigma_r$  (or  $\sigma_R$  in cylindrical coordinates) just outside the solar neighborhood is significantly smaller than the canonical value of  $\sim 150 \text{ km s}^{-1}$  in the solar neighborhood (Table 1). This incompatibility will be further discussed in §5.

The sample with  $g > 18$  contains the 437 faintest stars. Since the stars are all very far away, the non-radial components of the velocity ellipsoid are very poorly constrained. Note that the quoted errors may also be ill-determined because of departures from gaussianity for small eigenvalues. However, the essential result remains the same: the radial component of the velocity ellipsoid is  $\sim 100 \text{ km s}^{-1}$ .

Finally, to address concerns that the determination of the velocity ellipsoid may be contaminated by halo substructure, the last two lines of Table 2 show the results for all stars excluding the Sagittarius stream. This exclusion is conservatively accomplished by simply rejecting all BHB stars within 10 degrees of the great circle with pole  $(\ell, b) = (94, 11)$ , which approximates the Sagit-

tarius stream (Ivezić et al. 2003, Paper I). Since the Sagittarius stream is the most conspicuous substructure in our sample of BHB stars (Paper I), the stability of the velocity ellipsoid solution indicates that halo substructure does not appreciably influence the results.

#### 4. Monte Carlo simulations

An independent way of verifying the accuracy of the maximum likelihood technique is through Monte Carlo simulations. In case the geometry of the SDSS footprint (see Paper I) affects the analysis, we assemble 1170 artificial stars with the same angular coordinates and measured  $g$  magnitudes as the complete BHB sample, but with newly constructed velocities. For simplicity absolute magnitudes are assumed constant at 0.7. Only velocity ellipsoids aligned with spherical coordinates will be considered here. These Monte Carlo simulations perform the three-parameter fit to the velocity ellipsoid with  $\mathbf{v}_{\odot} = (10, 225, 7) \text{ km s}^{-1}$  and  $v_{\text{halo}} = 0 \text{ km s}^{-1}$ . Note, however, that the values of  $\mathbf{v}_{\odot}$  and  $v_{\text{halo}}$  are irrelevant here since they are first added to the stars’ velocities in construction, and then subtracted as known in the parameter determination.

We run 100 Monte Carlo simulations on each of four setups. The first setup does not consider magnitude or velocity errors; the second setup allows for  $\Delta m = 0.5$ ; the third assumes  $\Delta v = 30 \text{ km s}^{-1}$ . The fourth setup considers the magnitude and velocity errors as well as allowing for contamination.

The constructed set of artificial stars has known space positions, so it is straightforward to apply an assumed velocity ellipsoid to obtain a simulated three-dimensional space velocity for each star. Here we assume  $\sigma = (150, 100, 80) \text{ km s}^{-1}$  to strain the maximum likelihood analysis. The three-dimensional velocities are then projected onto the line of sight to each star to obtain  $v_{\text{los}}$ , and then the projections of  $\mathbf{v}_{\odot}$  and  $v_{\text{halo}}$  are subtracted to obtain  $v_r$ . This comprises the simulated data set for the first setup. To incorporate magnitude errors, the radial distances to the stars are shuffled, i.e. the  $g$  magnitudes are shifted by a gaussian error distribution of width  $\Delta m$ ,  $v_r$  is calculated as before, and then the  $g$  magnitudes are shifted back to their “observed” positions. Velocity errors are incorporated by adding an error to each observed  $v_r$ . To incorporate contamination, a fraction of stars are randomly flagged as disk stars. These stars are then assumed to be 2.5 times closer (2 mag) to the Sun than they would be if they were BHB stars. Their velocities are taken to be  $220 \text{ km s}^{-1}$  in the  $-\phi$  direction plus three random components from a *disk* velocity dispersion, which is assumed isotropic with components  $(20, 20, 20) \text{ km s}^{-1}$ . Dehnen & Binney (1998) find a non-isotropic disk velocity dispersion with components of the same order (depending on color), but our intent is to contaminate the simulated halo star population in a simple and controlled way.

Figure 3 shows the results of these Monte Carlo simulations with the four setups colored black (no errors), blue (magnitude errors), red (velocity errors), and green (magnitude and velocity errors with 10% contamination). As shown, the scatter in the results of the Monte Carlo simulations is comparable to the confidence regions shown in figure 2, so our error analysis is verified to be

reasonable. As in the analysis of the real data, the radial component of the velocity ellipsoid  $\sigma_r$  is very well constrained; one can also see anticorrelation between any two components. The black dots and blue dots occupy essentially the same region of parameter space; this verifies, independently of the method used in §3, that magnitude errors of the order  $\Delta m$  do not affect our results significantly.

As shown in Table 3, the mean determinations of  $\sigma$  over 100 Monte Carlo simulations recover the input values for the “no errors” case and the “magnitude errors only” case. It is also clear that velocity errors of scale  $\Delta v = 30 \text{ km s}^{-1}$  push the measured values higher by  $\sim 5 \text{ km s}^{-1}$  because the error adds in quadrature. This result is consistent with the independent determination in §3 which stated that with  $\Delta v = 30 \text{ km s}^{-1}$  the “true” values of the velocity ellipsoid (i.e., those measured using the analysis that allows for velocity errors) were  $\sim 5 \text{ km s}^{-1}$  lower than the “measured” values (not considering velocity errors). Finally, it is interesting that for the case which includes contamination by disk stars, the determination of  $\sigma_\phi$  increases while those of  $\sigma_r$  and  $\sigma_\theta$  both decrease. This is because the disk stars are constructed to travel primarily in the  $\phi$  direction.

However, the main conclusion to be gained from these Monte Carlo simulations is that the radial component of the velocity ellipsoid never strays too far from its correct value of  $150 \text{ km s}^{-1}$ , even allowing for errors such as contamination. Thus the maximum likelihood analysis is verified to be reliable and stable.

## 5. Summary and discussion

Applying maximum-likelihood methods to the line-of-sight velocities and photometric distances of BHB stars, we have modeled the kinematics of the relatively distant galactic halo. (The median distance of the sample is about 25 kpc.) No significant anisotropy of the velocity ellipsoid is detected. In a model aligned with spherical coordinates, for example,  $\sigma = (101.4, 97.7, 107.4) \text{ km s}^{-1}$ . However, the errors in  $\sigma_\theta$  and  $\sigma_\phi$  are much larger,  $\sim 15 - 20 \text{ km s}^{-1}$ , than that of  $\sigma_r$ , because of the great distances of most stars: that is, the Galactocentric radius  $r$  of most stars is more than twice that of the Sun, so that the direction of the line of sight is not far from radial despite the broad angular range of our sample. This result contrasts starkly and surprisingly with the radial anisotropy of halo velocities in the solar neighborhood ( $\sigma \sim (150, 100, 100) \text{ km s}^{-1}$ ; see Table 1). Our results are consistent, however, with the only other comparable study of distant halo field stars: Sommer-Larsen et al. (1997).

We are able to fit separately for the rotation speed of the halo ( $v_{\text{halo}}$ ) and the orbital velocity of the Sun, although the two are strongly covariant. The halo rotation is marginally consistent with zero at the one-sigma level, which is  $\sim 20 \text{ km s}^{-1}$ . The difference  $v_{\odot,y} - v_{\text{halo}} = 222.1 \pm 7.7 \text{ km s}^{-1}$  is more tightly constrained than either quantity separately. This is consistent with a non-rotating halo if one accepts the IAU recommendation for the local standard of rest,  $\mathbf{v}_{\text{LSR}} = 220 \text{ km s}^{-1}$  (Kerr & Lynden-Bell 1986) and Dehnen & Binney (1998)’s solar motion,  $\mathbf{v}_{\odot} - \mathbf{v}_{\text{LSR}} = (10, 5, 7) \text{ km s}^{-1}$ , although some authors have advocated a substantially smaller (Olling & Merrifield

1998) or larger (Uemura et al. 2000) value of the azimuthal component of  $\mathbf{v}_{\text{LSR}}$ . (If the solar rotation is substantially less than  $225 \text{ km s}^{-1}$ , then according to our results, the halo should counterrotate!) Our result is also statistically consistent with most of the studies cited in Table 1, although the latter seem to prefer a slight positive halo rotation. Note that what those studies actually measure is the mean velocity of local halo stars relative to the Sun; the values for  $v_{\text{halo}}$  in the fourth column of that table have been adjusted to  $V_{\odot} = 225 \text{ km s}^{-1}$  so that they can be compared directly to our result. Presumably,  $\mathbf{v}_{\text{LSR}}$  will soon be determined with exquisite accuracy by a variant of the classical visual-binary method applied to stars orbiting Sgr A\*, but accurate values are not in the public domain at the time of writing (Ghez et al. 2003; Salim & Gould 1999).

Of course, the measurement of  $v_{\text{halo}}$  depends upon the assumption that the halo rotation curve is flat; line-of-sight velocities would be unaffected by adding a solid-body component to the angular velocity of the halo, although proper motions would be (see below).

These are the main results of our study. It is likely that more science could be extracted from this sample, and completion of the SDSS will allow it to be enlarged. For the present, we simply highlight certain interesting features of the data that have not yet been thoroughly explored.

The distribution of  $v_{\text{los}}$  is plotted in figure 4 and beautifully follows a gaussian of width  $\sigma_{\text{los}} = 101.6 \pm 3.0 \text{ km s}^{-1}$ . The uncertainty quoted here is one-sigma statistical, to which should be added a similar systematic uncertainty pending better quantification of our measurement errors. An estimate of this systematic error is easily determined as  $\sigma_{\text{los}} - \sqrt{\sigma_{\text{los}}^2 - \Delta v^2} \approx 3.4 \text{ km s}^{-1}$  ( $\Delta v = 26 \text{ km s}^{-1}$  from Paper I). The line-of-sight velocities (figure 4) are about as gaussianly distributed as the number of stars would allow. This is consistent with (although not required by) the isotropy of the velocity ellipsoid that we find, since a strongly anisotropic ellipsoid, even if gaussian along each individual axis, would not produce an exact gaussian in an average over many lines of sight. Gaussianity could result from large observational errors, regardless of the intrinsic velocity distribution, if the errors were gaussian, but our errors seem not to be large enough to dominate the observed distribution (Paper I). By contrast, the distribution of transverse velocities of halo stars in the solar neighborhood is distinctly nongaussian, with a negative kurtosis (Popowski & Gould 1998). This is another indication that the local halo differs from the more distant halo probed by our BHB sample.

Another aspect of the data that could be thoroughly explored is the smoothness of the BHB phase-space distribution. The notion of a stellar velocity ellipsoid implicitly presumes that phase space is smoothly populated. If instead the distribution is very lumpy and the number of important lumps or streams is small, then statistical characterizations of *individual* halos, in particular that of the Galaxy, may not be meaningful. In cosmology, however, statistical descriptions are unavoidable. Current theory holds that galactic halos have been built up by accretion of lesser systems (Searle & Zinn 1978; Bullock, Kravtsov, & Weinberg 2001). Accreted gas joins galactic disks, and the details of its history are effaced by dissipation. Stars that form in these systems before they are accreted (and presumably also their dark matter), however, behave collisionlessly and preserve a

partial record of their origins. The structure of the stellar and dark-matter halos should be related. Helmi, White, & Springel (2003) conclude from a detailed analysis and scaling of cosmological simulations that the number of streams composing a halo similar to that of the Galaxy should be large, amounting to almost  $10^4$  within 25 kpc, and that most streams joined the Galaxy early on, allowing more time for phase mixing. The number of our BHB stars is much smaller than this, so that one might expect to find a smooth distribution. And yet we see structure in our sample that is consistent with the tidal stream of the Sagittarius Dwarf (Paper I), as previously delineated in SDSS data (Ivezić et al. 2000; Yanny & Newberg et al. 2000; Ibata et al. 2001a; Newberg & Yanny et al. 2002) and in a survey of carbon stars (Ibata et al. 2001b). Most of our results for the halo velocity ellipsoid are scarcely affected by excluding that part of the sample that lies close to the Sagittarius stream on the sky. In short, it is not yet clear whether the kinematics of the Galactic halo admit a statistical description. Larger samples of stars will be necessary to clarify this.

In Paper I, we used proper motions only as a check on the purity of our sample. Calibration against the QSOs shows that the proper motions of individual BHB stars in our sample are smaller than measurement errors by factors  $\sim 3 - 5$ , but statistical detection of the kinematics of the population as a whole should certainly be possible. Among other benefits, this would allow a direct constraint on the solid-body component of halo rotation and a further test of the isotropy of the velocity dispersions. Systematic errors in the proper motion data present many complexities, however, so we defer their analysis to a later paper. The quality of the USNO-B data should be appreciably better than that of the USNO-A, and one should probably use the former to determine the proper motions of SDSS objects.

Our BHB radial velocity data could be used to constrain the mass of the outer Galaxy. We have not yet attempted a serious dynamical analysis, partly in order to do full justice to the kinematics, but also because mass measurements rely more heavily on aspects of the data that are less certain: namely, the photometric distances and the completeness as a function of magnitude. However, since no kinematic information was used in the selection of the sample, we may assume that the velocities fairly represent the whole population of BHB stars, whose spatial density is often described as a powerlaw in Galactocentric radius,  $n \propto r^{-\alpha}$ , with exponent  $\alpha \approx 3.5$  (Kinman, Suntzeff, & Kraft 1994). In that case, to the extent that the dispersions are isotropic and constant with radius and rotation is negligible, and that the potential is spherical, Jeans' equations imply

$$v_{\text{circ}} \approx 187 \left( \frac{\alpha}{3.5} \right)^{1/2} \left( \frac{\sigma}{100 \text{ km s}^{-1}} \right), \quad (2)$$

$$M(r) \approx 2.0 \times 10^{11} \left( \frac{v_{\text{circ}}}{187 \text{ km s}^{-1}} \right)^2 \left( \frac{r}{25 \text{ kpc}} \right) M_{\odot}. \quad (3)$$

The value of  $v_{\text{circ}}$  so obtained, with  $\sigma \approx 100 \text{ km s}^{-1}$ , is substantially lower than the circular velocity in the vicinity of the Sun. Faced with similar evidence drawn from their own independent BHB sample, Sommer-Larsen et al. (1997) concluded that the tangential velocity dispersion of the halo probably rises beyond  $r \sim 20 \text{ kpc}$  so as to exceed the radial dispersion and be consistent with a constant circular velocity. At such distances, however, the tangential dispersions are very

poorly constrained by line-of-sight velocities without *a priori* assumptions about the potential (see Table 2). Rather than make such assumptions, one may prefer to await further direct evidence.

We thank A. Gould, B. Paczyński, R. Lupton, and J. Hennawi for helpful discussions, and M. Strauss for a close reading of a draft of this paper. GRK is grateful for generous research support from Princeton University and from NASA via grants NAG-6734 and NAG5-8083. Funding for the creation and distribution of the SDSS Archive has been provided by the Alfred P. Sloan Foundation, the Participating Institutions, the National Aeronautics and Space Administration, the National Science Foundation, the U.S. Department of Energy, the Japanese Monbukagakusho, and the Max Planck Society. The SDSS Web site is <http://www.sdss.org/>. The SDSS is managed by the Astrophysical Research Consortium (ARC) for the Participating Institutions. The Participating Institutions are The University of Chicago, Fermilab, the Institute for Advanced Study, the Japan Participation Group, The Johns Hopkins University, Los Alamos National Laboratory, the Max-Planck-Institute for Astronomy (MPIA), the Max-Planck-Institute for Astrophysics (MPA), New Mexico State University, the University of Pittsburgh, Princeton University, the United States Naval Observatory, and the University of Washington.

### A. The maximum likelihood technique

In this section we outline the maximum likelihood procedure used to determine the velocity ellipsoid of the Galactic halo.

Halo stars are assumed to have a gaussian velocity distribution whose principal axes align with spherical or cylindrical coordinates. In this appendix we assume the velocity of the Sun relative to the galactic center is known and subtracted from stars’ radial velocities, and that every star’s position in space is known exactly; see §2 for a discussion of magnitude and velocity errors. We define  $\mathbf{x}$  as the normalized heliocentric line-of-sight vector to the star, so that the line-of-sight velocity  $v_{\text{los}} = \mathbf{x} \cdot \mathbf{v}$  where  $\mathbf{v}$  is the true space velocity of the star. The three components of each of the vectors  $\mathbf{x}$ ,  $\mathbf{v}$ , and  $\boldsymbol{\sigma}$  should be thought of as projections along the principal axes of the velocity ellipsoid at the specific point in space. The probability  $\phi dv_{\text{los}}$  of observing a given star with a radial velocity between  $v_{\text{los}}$  and  $dv_{\text{los}}$  is expressed as an integral over the possible combination of true space velocities that would result in an observation between  $v_{\text{los}}$  and  $dv_{\text{los}}$ :

$$\phi(v_{\text{los}}) dv_{\text{los}} = \int_{-\infty}^{\infty} \int_{-\infty}^{\infty} \phi_1(v_1)\phi_2(v_2)\phi_3(v_3) dv_1 dv_2 dv_3 \quad (\text{A1})$$

where  $v_1$ ,  $v_2$ , and  $v_3$  are the components of the star’s velocity in the directions of the principal axes. Here  $\phi_i(v_i) dv = (2\pi\sigma_i^2)^{-1/2} \exp(-v_i^2/2\sigma_i^2) dv$  where  $\sigma_i$  is the component of the velocity ellipsoid in the  $i$  direction. Geometry dictates a relation between  $dv_{\text{los}}$  and the other infinitesimal quantities:  $dv_{\text{los}} = |x_i|dv_i$ . Also, the vector  $\mathbf{v}$  is constrained by  $v_{\text{los}}$  by the relation  $v_{\text{los}} = \mathbf{x} \cdot \mathbf{v}$  so finally our

integral becomes

$$\phi(v_{\text{los}}) dv_{\text{los}} = \frac{dv_{\text{los}}}{|x_1|} \int_{-\infty}^{\infty} \int_{-\infty}^{\infty} dv_2 dv_3 \phi_1 \left( \frac{1}{x_1} (v_{\text{los}} - x_2 v_2 - x_3 v_3) \right) \phi_2(v_2) \phi_3(v_3) \quad (\text{A2})$$

Here the integral integrates over the 2 and 3 directions, which is mathematically correct if  $x_1 \neq 0$ , but to avoid small-number numerical problems, in practice the code shuffles the indices as appropriate to ensure that the largest component of  $\mathbf{x}$  is placed in the denominator. The value of the integral is

$$\begin{aligned} \phi(v_{\text{los}}) &= \frac{1}{\Gamma} \exp \left( \frac{-v_{\text{los}}^2}{2\hat{\sigma}_{\text{los}}^2} \right) & (\text{A3}) \\ \frac{1}{2\hat{\sigma}_{\text{los}}^2} &= C' - B'^2/4A' & \Gamma &= |x_1| \sigma_1 \sigma_2 \sigma_3 \sqrt{8\pi AA'} \\ A' &= -\frac{x_3^2}{2\sigma_1^2 x_1^2} (D-1) + \frac{1}{2\sigma_3^2} & B' &= \frac{x_3}{\sigma_1^2 x_1^2} (D-1) & C' &= -\frac{1}{2\sigma_1^2 x_1^2} (D-1) \\ A &= \frac{1}{2\sigma_2^2} + \frac{x_2^2}{2\sigma_1^2 x_1^2} & D &= \frac{\sigma_2^2 x_2^2}{\sigma_1^2 x_1^2 + \sigma_2^2 x_2^2}. \end{aligned}$$

Note that at a given position, stars are most likely to be found at zero velocity (with respect to the galactic center) but have a characteristic velocity dispersion  $\hat{\sigma}_{\text{los}}$ , which is a function of the geometry of the stars with respect to the Sun and of  $\boldsymbol{\sigma}$ . Since the probability of observing a set of stars with known space locations and observed line-of-sight velocities is the product of the individual probabilities, the log-likelihood is

$$\mathcal{L}(\boldsymbol{\sigma}) = -\frac{N}{2} \ln (8\pi \sigma_1^2 \sigma_2^2 \sigma_3^2) + \sum \left[ \left( \frac{B'^2}{4A'} - C' \right) v_{\text{los}}^2 - \frac{1}{2} \ln (x_1^2 AA') \right] \quad (\text{A4})$$

where the summation is over all observed stars. Assuming a uniform prior (Lupton 1993), we find the maximum of  $\mathcal{L}(\sigma_1, \sigma_2, \sigma_3)$  to determine the most likely values of the velocity ellipsoid  $\boldsymbol{\sigma}$ .

If quantities such as the velocity of the Sun with respect to the Galactic center or the bulk rotation velocity of the halo are free parameters, they can be determined from this maximum-likelihood estimate. These quantities affect  $v_{\text{los}}$  for every star, so it is straightforward to extrapolate equation A4 to  $\mathcal{L} = \mathcal{L}(\boldsymbol{\sigma}, \mathbf{v}_{\odot}, v_{\text{halo}})$ .

## REFERENCES

- Abramowitz, M. & Stegun, I. A. 1972, Handbook of Mathematical Functions (New York: Dover)
- Armandroff, T. E. 1989, *AJ*, 97, 375
- Binney, J. & Merrifield, M. 1998, Galactic astronomy (Princeton, NJ: Princeton University Press)
- Bullock, J. S., Kravtsov, A. V., & Weinberg, D. H. 2001, *ApJ*, 548, 33
- Carney, B. W. & Latham, D. W. 1986, *AJ*, 92, 60
- Chiba, M. & Beers, T. C. 2000, *AJ*, 119, 2843
- Dehnen, W. & Binney, J. J. 1998, *MNRAS*, 298, 387
- Frenk, C. S. & White, S. D. M. 1980, *MNRAS*, 193, 295
- Ghez, A. M. et al. 2003, *ApJ*, 586, L127
- Gould, A. 2003, *ApJ*, 583, 765
- Helmi, A., White, S. D. M., & Springel, V. 2003, *MNRAS*, 339, 834
- Ibata, R., Irwin, M., Lewis, G. F., & Stolte, A. 2001a, *ApJ*, 547, L133
- Ibata, R., Lewis, G. F., Irwin, M., Totten, E., & Quinn, T. 2001b, *ApJ*, 551, 294
- Ivezić, Ž. et al. 2003, in the Proceedings of Milky Way Surveys: The Structure and Evolution of Our Galaxy, in press
- Ivezić, Ž. et al. 2000, *AJ*, 120, 963
- Kerr, F. J. & Lynden-Bell, D. 1986, *MNRAS*, 221, 1023
- Kinman, T. D., Suntzeff, N. B., & Kraft, R. P. 1994, *AJ*, 108, 1722
- Layden, A. C., Hanson, R. B., Hawley, S. L., Klemola, A. R., & Hanley, C. J. 1996, *AJ*, 112, 2110
- Lupton, R. 1993, Statistics in theory and practice (Princeton, NJ: Princeton University Press)
- Morrison, H. L., Flynn, C., & Freeman, K. C. 1990, *AJ*, 100, 1191
- Newberg, H. J. & Yanny, B. et al. 2002, *ApJ*, 569, 245
- Norris, J. 1986, *ApJS*, 61, 667
- Norris, J., Bessell, M. S., & Pickles, A. J. 1985, *ApJS*, 58, 463
- Olling, R. P. & Merrifield, M. R. 1998, *MNRAS*, 297, 943

- Pier, J. R. 1984, *ApJ*, 281, 260
- Popowski, P. & Gould, A. 1998, *ApJ*, 506, 259
- Ratnatunga, K. U. & Freeman, K. C. 1989, *ApJ*, 339, 126
- Ratnatunga, K. U. & Yoss, K. M. 1991, *ApJ*, 377, 442
- Reid, M. J. 1993, *ARA&A*, 31, 345
- Ryan, S. G. & Norris, J. E. 1991, *AJ*, 101, 1835
- Salim, S. & Gould, A. 1999, *ApJ*, 523, 633
- Searle, L. & Zinn, R. 1978, *ApJ*, 225, 357
- Sirko, E. et al. 2003, *AJ*, submitted (Paper I)
- Sommer-Larsen, J., Beers, T. C., Flynn, C., Wilhelm, R., & Christensen, P. R. 1997, *ApJ*, 481, 775
- Uemura, M., Ohashi, H., Hayakawa, T., Ishida, E., Kato, T., & Hirata, R. 2000, *Pub. Astron. Soc. Japan*, 52, 143
- Woolley, R. 1978, *MNRAS*, 184, 311
- Yanny, B. & Newberg, H. J. et al. 2000, *ApJ*, 540, 825
- Zinn, R. 1985, *ApJ*, 293, 424

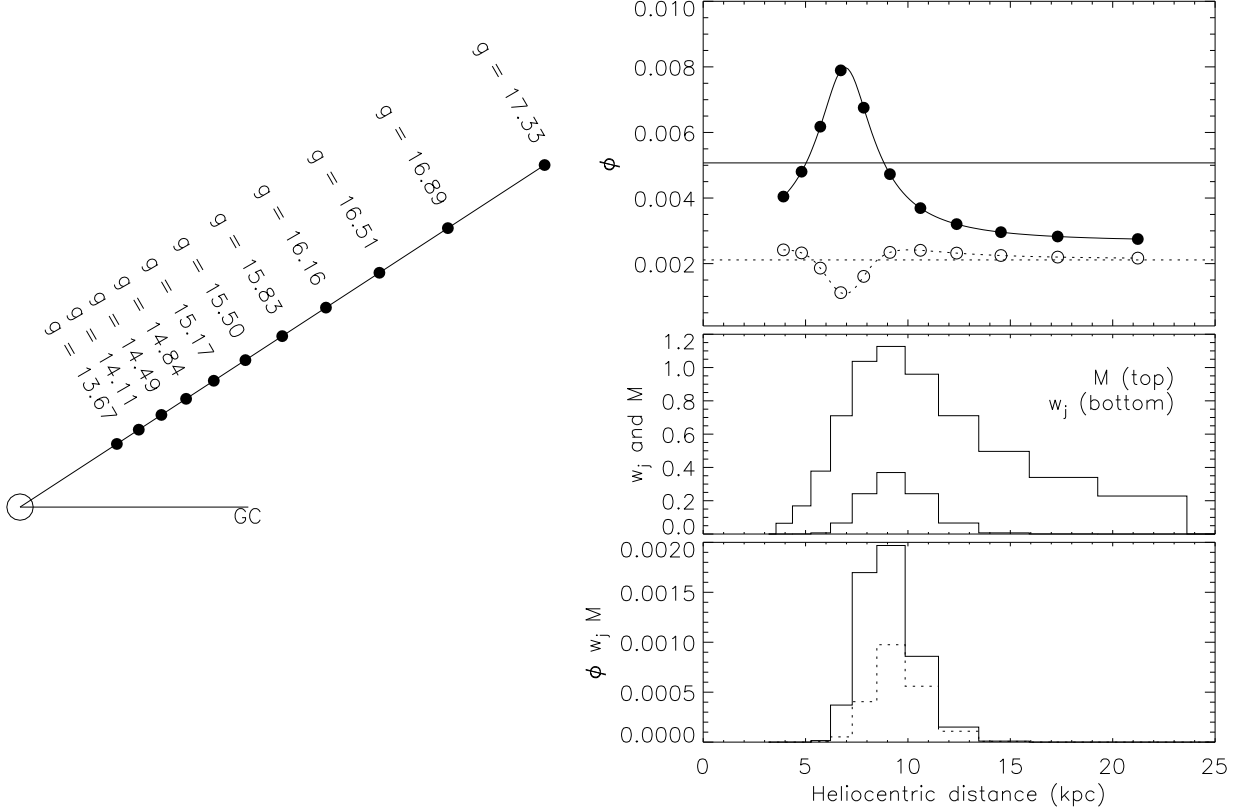


Fig. 1.— An illustration of the technique used to incorporate magnitude errors into the maximum likelihood analysis, for two artificial stars. The two stars are at the same measured position:  $(l, b) = (0, 30)$ ,  $g = 15.5$ , and absolute magnitude  $0.7$ . Magnitude errors mean that the stars could be located anywhere along the line of sight indicated in the left panel. One star has  $v_{\text{los}} = 0 \text{ km s}^{-1}$  and the other has  $v_{\text{los}} = 100 \text{ km s}^{-1}$ . Here we assign a model with  $\sigma = (150, 50, 100) \text{ km s}^{-1}$  in spherical coordinates, and neglect any velocity of the Sun with respect to the galactic center. The upper right panel plots the probability density of the existence of each star with given  $v_{\text{los}}$  at the position given by the abscissa (see equation A3). The solid line represents the stationary star, and the dotted line represents the receding star. The middle panel shows the weights of Gauss-Hermite integration  $w_j$  (bottom line) and the Malmquist factor  $M(r)$  (top line), as described in the text, which are then multiplied to  $\phi$  to arrive at the solid (stationary star) and dotted (receding star) lines in the bottom panel. The values of  $\phi w_j M$  are summed over the eleven abscissae, and plotted in the upper right panel as the horizontal solid and dotted lines, for the stationary and receding stars respectively.

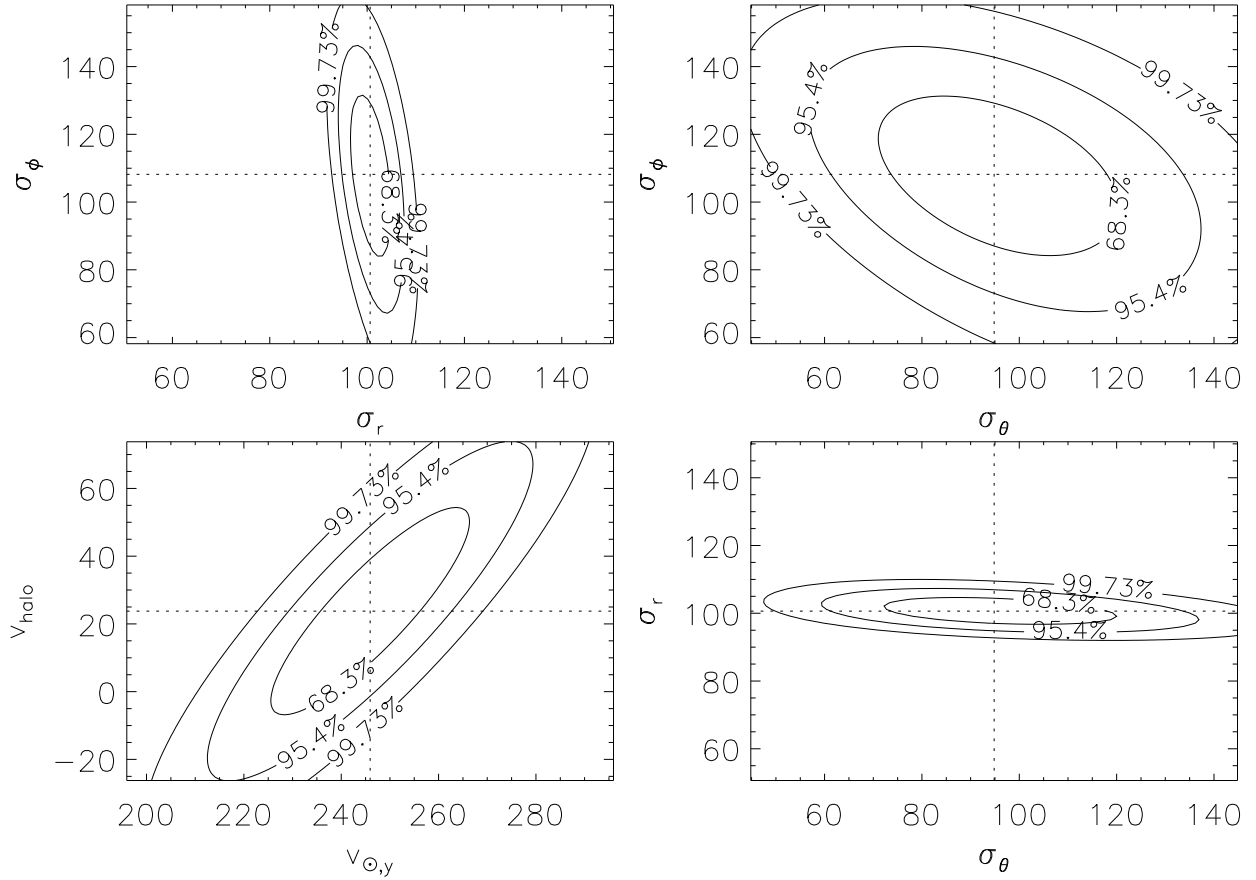


Fig. 2.— Approximate confidence regions for the components of the velocity ellipsoid determined from the complete BHB sample (1170 stars) in spherical coordinates, demonstrating  $\sigma_r$  is very well constrained and that each component is anticorrelated with the other two. In the lower left panel, the confidence regions for the halo rotation and the solar velocity in the  $+y$  direction are shown.

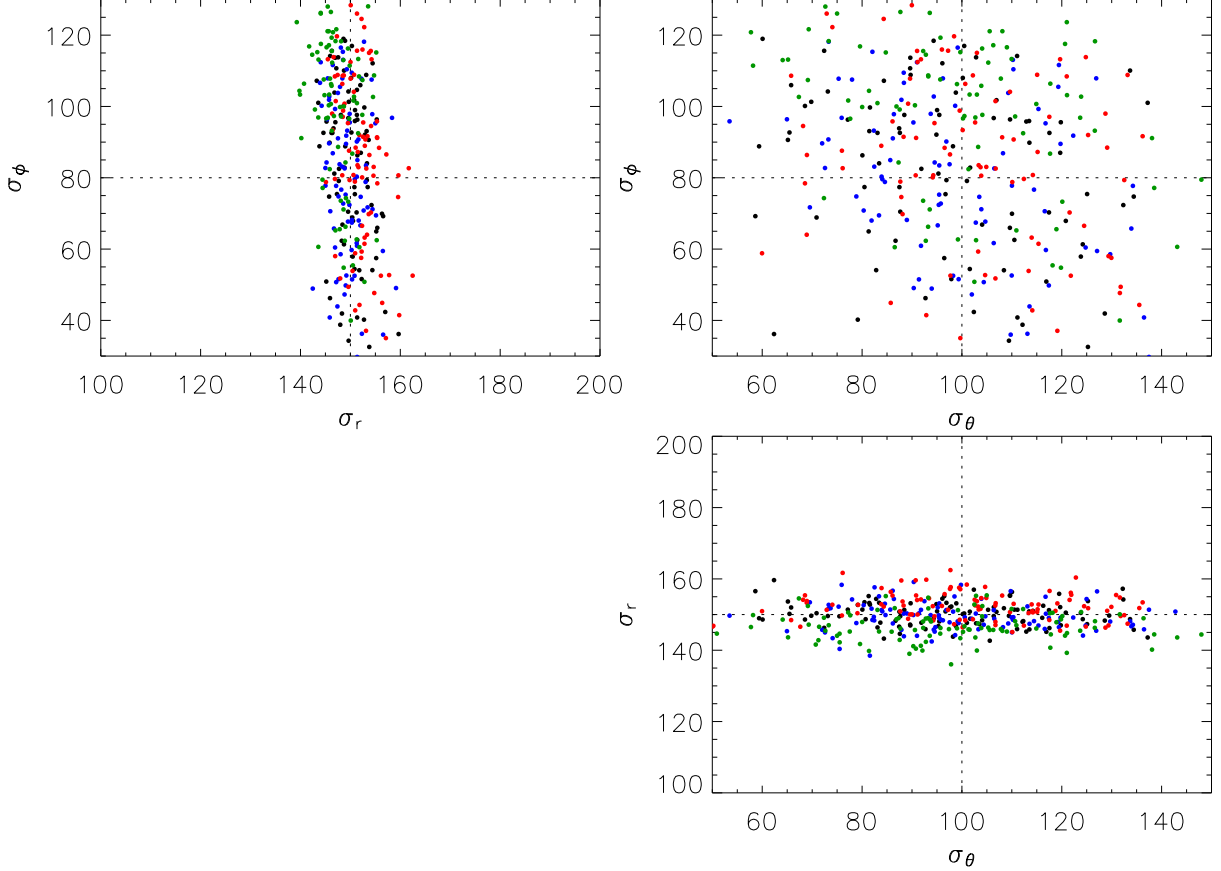


Fig. 3.— Each dot represents the results from a Monte Carlo simulation with input  $\sigma = (150, 100, 80) \text{ km s}^{-1}$  in spherical coordinates. Black dots assume no magnitude or velocity errors. Blue dots assume the stars are not really at the heliocentric radial positions observed, with an error  $\Delta m = 0.5$ . Red dots assume the positions are accurate, but that the velocities are measured with an error  $\Delta v = 30 \text{ km s}^{-1}$ . Green dots assume magnitude and velocity errors, as well as a 10% contamination from disk stars. This plot provides evidence that the error estimate as shown in figure 2 is accurate. Additionally, the radial component of the velocity ellipsoid is very well constrained, as in the analysis of the real data. One can also make out slight anticorrelations between all three parameters, as with the real data. Magnitude errors (blue dots) have no perceivable effect on the parameter determinations of the velocity ellipsoid. Velocity errors of  $30 \text{ km s}^{-1}$  (red dots) introduce a small positive shift of order  $\sim 5 \text{ km s}^{-1}$  to each of the three components of the velocity ellipsoid, which is most easily seen in the radial component. Contamination (green dots) shifts  $\sigma_\theta$  and  $\sigma_r$  to lesser values and  $\sigma_\phi$  to larger values, as expected; also see Table 3.

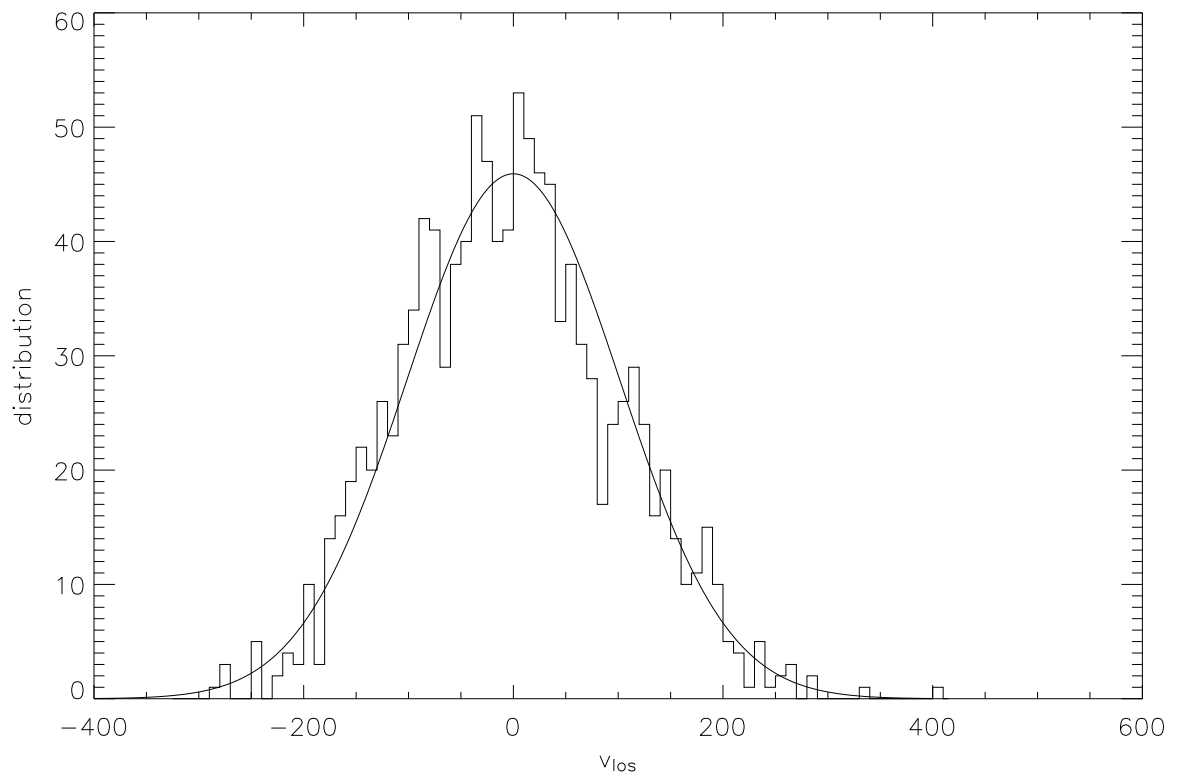


Fig. 4.— Histogram of  $v_{\text{los}} = v_r + \mathbf{x} \cdot \mathbf{v}_{\odot}$  ( $\mathbf{v}_{\odot} = (10, 5, 7) \text{ km s}^{-1}$  (Dehnen & Binney 1998)), with a gaussian of width  $\sigma_{\text{los}} = 101.6$ .

Table 1. Recent results for the local halo velocity ellipsoid. The velocity ellipsoid components  $(R, \phi, z)$  correspond to galactocentric cylindrical coordinates and point radially (outwards), retrograde to galactic rotation, and towards the north galactic pole, respectively. Entries in the fourth column assume  $\mathbf{v}_{\text{LSR}} = (0, 220, 0) \text{ km s}^{-1}$  and  $\mathbf{v}_{\odot} - \mathbf{v}_{\text{LSR}} = (10, 5, 7) \text{ km s}^{-1}$ .

$\sigma_R$	$\sigma_\phi$	$\sigma_z$	$v_{\text{halo}}$	comments	source
$125 \pm 11$	$96 \pm 9$	$88 \pm 7$	—	$[\text{Fe}/\text{H}] < -1.2; V \leq 11 \text{ mag}$	Norris, Bessell, & Pickles (1985)
$131 \pm 6$	$106 \pm 6$	$85 \pm 4$	$32 \pm 10$	$[\text{Fe}/\text{H}] < -1.2$	Norris (1986)
$154 \pm 18$	$102 \pm 27$	$107 \pm 15$	$7 \pm 23$	$[\text{Fe}/\text{H}] < -1.5; \text{ red giants}$	Carney & Latham (1986)
$133 \pm 8$	$98 \pm 13$	$94 \pm 6$	$21 \pm 15$	$D \sim 4 \text{ kpc}, [\text{Fe}/\text{H}] < -1.6$	Morrison, Flynn, & Freeman (1990)
$145 \pm 10$	$100 \pm 10$	—	$30 \pm 10$	$[\text{Fe}/\text{H}] < -1.5; \text{ kin. sel. subdwarfs}$	Ryan & Norris (1991)
—	—	$54 \pm 4$	—	metal-poor RGs, $D < 4 \text{ kpc}$	Ratnatunga & Yoss (1991)
$168 \pm 13$	$102 \pm 8$	$97 \pm 7$	$15 \pm 12$	RR Lyr: stat- $\pi$ & $v_{\text{los}}$	Layden et al. (1996)
$151 \pm 9$	$121 \pm 7$	$103 \pm 6$	$13 \pm 10$	$ Z  < 4 \text{ kpc}, [\text{Fe}/\text{H}] < -2.2$	Chiba & Beers (2000)
$162 \pm 1$	$106 \pm 2$	$89 \pm 2$	—	stat $\pi, \langle V \rangle - V_{\odot} \equiv -216.6 \text{ km s}^{-1}$	Gould (2003)

Table 2. Results

criteria	$N_{\text{stars}}$	c.s.	errors	$v_{\odot,x}$	$v_{\odot,y}$	$v_{\odot,z}$	$v_{\text{halo}}$	$\sigma_r$ (sph), $\sigma_R$ (cyl)	$\sigma_\theta$ (sph), $\sigma_\phi$ (cyl)	$\sigma_\phi$ (sph), $\sigma_z$ (cyl)
all	1170	sph	0	10.0	225.0	7.0	0.0	$101.4 \pm 2.8(2.5)$	$97.7 \pm 16.4(14.5)$	$107.4 \pm 16.5(13.9)$
all	1170	sph	0	10.0	225.0	7.0	$-6.0 \pm 10.2(10.2)$	$101.4 \pm 2.8(2.5)$	$97.9 \pm 16.6(14.5)$	$107.9 \pm 16.6(13.9)$
all	1170	sph	0	$4.8 \pm 6.8(6.5)$	$245.9 \pm 13.6(6.7)$	$-7.2 \pm 4.0(3.8)$	$23.8 \pm 20.2(10.1)$	$100.6 \pm 2.8(2.4)$	$94.8 \pm 16.6(14.6)$	$108.2 \pm 16.5(13.8)$
all	1170	sph	m	10.0	225.0	7.0	0.0	$101.5 \pm 2.8(2.5)$	$102.1 \pm 18.0(15.1)$	$103.5 \pm 18.2(14.7)$
all	1170	sph	m/v	10.0	225.0	7.0	0.0	$96.9 \pm 3.0(2.6)$	$97.5 \pm 18.8(15.8)$	$99.1 \pm 19.0(15.3)$
all	1170	cyl	0	10.0	225.0	7.0	0.0	$98.7 \pm 7.7(5.7)$	$104.7 \pm 16.8(14.1)$	$102.8 \pm 5.2(3.3)$
all	1170	cyl	m	10.0	225.0	7.0	0.0	$99.2 \pm 7.8(5.7)$	$102.1 \pm 17.9(14.8)$	$102.9 \pm 5.2(3.3)$
all	1170	cyl	m/v	10.0	225.0	7.0	0.0	$94.5 \pm 8.1(6.0)$	$97.6 \pm 18.7(15.5)$	$98.5 \pm 5.4(3.5)$
$g < 18$	733	sph	0	10.0	225.0	7.0	0.0	$99.4 \pm 4.3(3.4)$	$100.0 \pm 17.2(14.7)$	$110.5 \pm 17.1(13.7)$
$g < 18$	733	cyl	0	10.0	225.0	7.0	0.0	$97.2 \pm 9.6(7.6)$	$109.1 \pm 18.0(13.8)$	$100.9 \pm 6.5(4.3)$
$g < 16$	227	sph	0	10.0	225.0	7.0	0.0	$105.4 \pm 10.9(8.2)$	$85.7 \pm 16.9(14.6)$	$117.6 \pm 24.5(18.2)$
$g < 16$	227	cyl	0	10.0	225.0	7.0	0.0	$108.8 \pm 19.7(16.2)$	$122.0 \pm 23.8(17.5)$	$94.1 \pm 12.5(8.3)$
$g > 18$	437	sph	0	10.0	225.0	7.0	0.0	$103.2 \pm 6.6(3.6)$	$28.6 \pm 1013.4(741.5)$	$113.8 \pm 211.2(140.1)$
$g > 18$	437	cyl	0	10.0	225.0	7.0	0.0	$99.7 \pm 13.4(8.6)$	$113.3 \pm 207.5(142.0)$	$104.5 \pm 10.4(5.5)$
excl. Sgr	775	sph	0	10.0	225.0	7.0	0.0	$100.6 \pm 3.6(3.0)$	$89.9 \pm 34.2(26.9)$	$106.8 \pm 19.5(14.7)$
excl. Sgr	775	cyl	0	10.0	225.0	7.0	0.0	$96.3 \pm 9.5(7.1)$	$102.1 \pm 18.8(15.2)$	$102.6 \pm 6.3(4.1)$

Note. — The criteria used to select subsamples from the entire sample of 1170 BHB stars are listed in the first column. The next three columns indicate the number of stars in the subsample, the coordinate system used, and whether magnitude or velocity errors were considered in the maximum likelihood analysis. The quoted errors not in parentheses are considering correlations among the parameters; the errors in parentheses do not consider correlations.

Table 3. Mean and rms of determinations for  $\sigma$  over 100 Monte Carlo simulations for four cases

error	color in figure 3	mean			rms		
		$\sigma_r$	$\sigma_\theta$	$\sigma_\phi$	$\sigma_r$	$\sigma_\theta$	$\sigma_\phi$
0	black	150.2	98.0	73.7	3.4	19.7	35.6
m	blue	149.5	98.7	73.7	3.9	18.3	35.4
v	red	152.3	101.1	79.3	3.8	19.5	35.9
m/v/c	green	146.6	96.8	104.7	4.0	20.5	30.7

Note. — The type of error(s) considered is indicated in the leftmost column: “0,” “m,” “v,” and “c” refer to no error, magnitude error, velocity error, and contamination, respectively. Compare the mean values of  $\sigma$  to the input to the simulation of  $(150, 100, 80) \text{ km s}^{-1}$ .